

Causal representation learning from network data

Jifan Zhang^{*1}, Michelle M. Li^{*2}, Elena Zheleva³

¹Northwestern University

²Harvard Medical School

³University of Illinois Chicago

Abstract

Causal disentanglement from soft interventions is identifiable under the assumptions of linear interventional faithfulness and availability of both observational and interventional data. Previous research has looked into this problem from the perspective of i.i.d. data. Here, we develop a framework, GRACE-VAE, for non-i.i.d. settings, in which structured context in the form of network data is available. GRACE-VAE integrates discrepancy-based variational autoencoders with graph neural networks to jointly recover the true latent causal graph and intervention effects. We show that the theoretical results of identifiability from i.i.d. data hold in our setup. We also empirically evaluate GRACE-VAE against state-of-the-art baselines on three genetic perturbation datasets to demonstrate the impact of leveraging structured context for causal disentanglement.

Introduction

Discovering the causal factors underlying data and how they influence each other is a key challenge in machine learning. Early disentangled representation learning methods have aimed to learn latent features that correspond to distinct generative factors, typically assuming that these factors are statistically independent (Higgins et al. 2018; Kumar, Sattigeri, and Balakrishnan 2017; Higgins et al. 2017). However, this assumption rarely holds in real-world scenarios, where generative factors often exhibit intricate dependencies. This realization has led to causal disentanglement approaches, which relax the independence assumption by modeling latent factors as nodes in a causal graph that can influence each other, i.e. the structural causal model (SCM). Recent works have begun learning such causal representations from data, for instance, by integrating SCM constraints into variational autoencoders (VAEs) (Yang et al. 2021; Zhang et al. 2023). These methods show that with appropriate data (including interventions) and assumptions, one can recover the latent causal model up to equivalence and predict intervention outcomes. Notably, Zhang et al. (2023) prove that even when the true causal variables are unobserved, a combination of observational and interventional data is sufficient to identify the latent causal directed acyclic graph (DAG) up to permutations of equivalent factors and to accurately extrapolate to

novel interventions. Such progress provides a foundation for causal representation learning in complex settings.

While causal disentanglement has advanced for i.i.d. data, many real-world data come in the form of network data with rich relational structure among the entities. Examples include social networks, where users are connected by friendships and hidden traits may influence their behaviors, and biological networks, where genes or proteins may interact via unobserved regulatory factors. In such cases, the observed variables \mathbf{X} are nodes connected by various relations (e.g., friendship, genetic interactions) and there may exist additional nodes \mathbf{H} (e.g., communities, biological pathways) that group the nodes and mediate these relations. However, existing causal representation learning methods largely ignore relational structure. They typically assume a flat data distribution and do not exploit known links between the entities. Conversely, graph-based inference methods in the literature often assume that the causal graph is fully/partially known (Feng, Zhang, and Yang 2023; Sanchez-Martin, Rateike, and Valera 2021) or consider only observable interventions on known nodes (Khemakhem et al. 2021). This leaves a significant gap: There is no general framework to learn a latent causal model from data that is relational nor can handle the realistic setting where the intervened variables are latent and unknown.

In this paper, we introduce a novel approach, Graph-Aware Causal Effects Variational AutoEncoder (GRACE-VAE), that combines graph neural networks with deep generative modeling to discover latent causal factors from network data enriched with interventions. At a high level, GRACE-VAE extends the VAE framework to incorporate an external network data’s structure among the entities. The encoder of GRACE-VAE is a graph neural network (GNN) that processes the heterogeneous network data of observed nodes (\mathbf{X} -entities), their observed group nodes (\mathbf{H} -entities), and various relationships between them. This GNN-based encoder passes messages along the observed edges, capturing structural context (e.g., connectivity patterns and neighbor attributes) to produce enriched embeddings for the \mathbf{X} nodes. These structure-aware embeddings are then fed into a variational inference network to approximate the posterior over latent variables. By doing so, the encoder infuses information from the network into the inferred latent representation, biasing the model towards explanations consistent with

^{*}These authors contributed equally.

the relational patterns. The decoder of GRACE-VAE instantiates an SCM over the latent variables. In particular, the decoder learns a DAG that captures the hypothesized causal structure among the latent factors. Interventions are modeled through a two-stage process. First, an intervention encoder maps each intervention indicator to a soft selection over latent variables and a proposed mechanism modification. Then, the decoder applies this modification by altering the causal mechanism of the selected latent variable, while leaving others unchanged. GRACE-VAE simultaneously learns: (1) the latent causal graph G , (2) the correspondence of interventions to latent targets via the intervention encoder’s assignments, and (3) a generative model capable of simulating interventional outcomes on the observed network. This work has **three key contributions**:

- We propose a framework for latent causal discovery that leverages structured context. GRACE-VAE, a variational graph autoencoder for causal disentanglement, jointly learns a latent causal graph and intervention effects that are informed by prior knowledge (via heterogeneous network data). Unlike existing methods that assume a given causal graph, fully observed variables, or independent observations, GRACE-VAE discovers the latent causal structure, guided by both network connectivity and intervention data.
- We show that our method, GRACE-VAE, inherits identifiability guarantees for causal representation learning (Zhang et al. 2023). In other words, GRACE-VAE’s learned causal model is theoretically identifiable up to equivalence under the assumptions of linear interventional faithfulness and conditional independence.
- Through comprehensive experiments with 3 benchmark datasets on genetic perturbations, we empirically demonstrate that GRACE-VAE reliably recovers the true latent causal graph and outperforms state-of-the-art baselines on predicting intervention outcomes for unseen perturbation combinations. Ablations on GRACE-VAE show that both the graph-based encoder and the causal decoder are crucial to its success; removing either component degrades both structure learning and predictive accuracy.

Overall, GRACE-VAE offers a new approach to uncovering latent causal factors in complex network systems, pushing the state of the art in both causal discovery and graph representation learning. It addresses a critical gap by unifying relational information and intervention-based causal inference, leading to more reliable causal analysis.

Related Works

Causal disentanglement learning

The concept of disentangled representation is formally defined by Higgins et al. (2018). A representation is considered disentangled if it can be decomposed into independent features such that altering a single factor of the input data affects only one corresponding feature. Most disentangled representation learning methods are based on generative models, particularly VAEs (Kumar, Sattigeri, and Balakrishnan 2017; Higgins et al. 2017; Zhu, Xu, and Tao 2021). VAEs

approximate the unknown true posterior $p(z|x)$ using a variational posterior $q(z|x)$. To enhance disentanglement, researchers have introduced various regularization techniques to the original VAE loss function. For instance, β -VAE (Higgins et al. 2017) incorporates a penalty coefficient into the Evidence Lower Bound (ELBO) loss to enforce a stronger independence constraint on the posterior distribution $q(z|x)$.

Some studies have disagreed with the independence assumption and propose causal disentanglement learning, assuming that the generating factors of the observable data are causally influenced by the group of confounding factors (Suter et al. 2019). SCM describes causal relationships among generating factors (Pearl 2000). Numerous studies have investigated methods for identifying latent causal graphs by maximizing log-likelihood scores (Chickering 2002; Cussens 2020; Solus, Wang, and Uhler 2021; Raskutti and Uhler 2018). Extensive research on causal disentanglement learning have focused on the discovery of causality from observational data (Yang et al. 2021; Kong et al. 2023; Buchholz et al. 2024; Varici et al. 2023). Yang et al. (2021) propose CausalVAE, implementing the causal disentanglement process introduced by Suter et al. (2019). Varici et al. (2023) examine the identifiability of nonparametric latent SCMs under linear mixing, with the assumption of exactly one intervention per latent node. Buchholz et al. (2024) investigate the identifiability of linear latent SCMs under nonparametric mixing, considering both hard and soft interventions within a framework of linear SCMs with additive Gaussian noise. Zhang et al. (2023) study identifiability for soft interventions and offers a learning algorithm based on VAE without any structural restriction on the map from latent to observed variables. GRACE-VAE builds upon CM-VAE (Zhang et al. 2023) to incorporate structured context via a graph neural network.

Variational autoencoders & graph neural networks

GNNs excel in encoding the topology in network data, while VAEs provide a principled framework for learning latent representations through probabilistic inference. The integration of these approaches has yielded powerful generative models for network data. Kipf and Welling (2016) introduce the Variational Graph Autoencoder (VGAE), which incorporates Graph Convolutional Networks (GCNs) into the VAE framework for unsupervised graph learning.

GNNs and VGAEs have since been used for causal discovery (Khemakhem et al. 2021; Sanchez-Martin, Rateike, and Valera 2021; Tao, Yu, and Li 2024). Khemakhem et al. (2021) propose CAREFL, an autoregressive normalizing flow for causal discovery and inference on bivariate networks. However, their evaluation only considers interventions on root nodes, which simplifies to mere conditioning on those variables. Tao, Yu, and Li (2024) design a VGAE for intervention target estimation that can concurrently learn across diverse causal graphs and sets of intervention targets in a self-supervised mode. Sanchez-Martin, Rateike, and Valera (2021) propose VACA, a class of variational graph autoencoders for causal inference, utilizing GNNs to encode the causal graph information. Feng, Zhang, and Yang (2023) propose CCVGAE to obtain optimal dis-

entangled latent representations and conduct link prediction for the causal graph given partial causal graph structures. However, their settings (Feng, Zhang, and Yang 2023; Sanchez-Martin, Rateike, and Valera 2021) assume that a causal graph over the variables is given, which differs from our setting in which the intervened variables are not observable and the DAG for the latent intervened variables is learned.

Problem Setup

Consider a heterogeneous network data composed of two entity types: entities $\mathbf{X} = (X_1, X_2, \dots, X_d)$ and entities $\mathbf{H} = (H_1, H_2, \dots, H_m)$. Multiple relational edges \mathbf{E} connect these entities, including edges e_{XX} between X , edges e_{HH} between H , and edges e_{XH} across the two entity types. These edges are captured by the adjacency structure A_{XX}, A_{HH}, A_{XH} . Underlying these entities, we posit that latent variables $\mathbf{U} = (U_1, U_2, \dots, U_p)$ drive the generation of X through an unknown deterministic function f such that $\mathbf{X} = f(\mathbf{U})$. Denote P_X as the induced distribution over \mathbf{X} .

Denote P_U as the joint distribution for \mathbf{U} , which can be factorized according to an unknown DAG G with p nodes representing $\{U_1, U_2, \dots, U_p\}$. G and P_U are faithful to each other (i.e., every conditional independence that holds in P_U corresponds exactly to a d -separation in G , and vice versa). Mathematically, $\mathbf{U} \sim P_U = \prod_{i=1}^p P(U_i \mid U_{\text{parent}_G(i)})$, where $\text{parent}_G(i) = \{j \in [p] : U_j \rightarrow U_i\}$ represents the index set of the parents of U_i in G .

We focus on single-node soft interventions applied to latent variables. Specifically, under an intervention I targeting a node U_i , the original joint distribution P_U is altered to an interventional distribution P_U^I . This intervention modifies only the conditional distribution of the target node, replacing $P(U_i \mid U_{\text{parent}_G(i)})$ with a new conditional distribution $P^I(U_i \mid U_{\text{parent}_G(i)})$, while preserving the conditional distributions of all other (non-target) nodes. Formally, the factorization of the interventional distribution P_U^I is given by $P_U^I = \prod_{i=1}^p P^I(U_i \mid U_{\text{parent}_G(i)})$, where $P^I(U_j \mid U_{\text{parent}_G(j)}) = P(U_j \mid U_{\text{parent}_G(j)})$ for all non-target node $U_j \neq U_i$. Denote the induced interventional distribution over \mathbf{X} as P_X^I .

We study the setting in which both observational and interventional data are available. Let $D^{(0)}$ denote the observational dataset and $\{D^{(k)}\}_{k=1,2,\dots,K}$ represent the interventional dataset generated under intervention I_k . Each dataset contains observations of node-level features for the observable entity \mathbf{X} , the nodes in \mathbf{H} , and the edge structures A_{XX}, A_{HH}, A_{XH} describing relationships both within and between the entities \mathbf{X}, \mathbf{H} . We assume that the features of \mathbf{H} are not available. To ensure identifiability under the most challenging conditions, we assume that each latent variable is subject to at least one intervention. This assumption aligns with the identifiability requirement established for linear structural causal models, i.e., one intervention per node for recovery when one does not assume prior knowledge of the target of interventions I_1, \dots, I_K (Squires et al. 2023).

To summarize, the features of entities \mathbf{H} , the latent variables \mathbf{U} , their dimensionality p , the causal graph G , and

the intervention targets of I_1, \dots, I_K are assumed to be unknown throughout the process. Given observed datasets $D^{(0)}, D^{(1)}, \dots, D^{(K)}$, our objective is to infer the full latent causal graph G , assign every intervention to its latent target, and accurately predict the effect of arbitrary future interventions on \mathbf{X} .

Model: GRACE-VAE

We propose a novel model, GRACE-VAE, for end-to-end discovery of latent causal graphs from heterogeneous network data and improved prediction of intervention effects on the observed system. Here, we describe the VAE framework for causal learning, the graph-aware encoder, the causal decoder, and the learning objective. The complete architecture of GRACE-VAE is illustrated in Figure 1.

VAE framework for causal learning

We adopt the VAE framework as the backbone for GRACE-VAE. Widely adopted in prior research on causal disentanglement (Zhang et al. 2023; Lippe et al. 2022; Brehmer et al. 2022), the VAE enables a theoretically grounded and robust optimization process, with the advantages of scalability, flexibility in the choice of components. Our VAE has a latent prior $p(Z)$ and a decoder $p_\theta(X|Z)$ whose likelihood reconstructs \mathbf{X} from the latent vector \mathbf{Z} . An inference network, also known as the encoder, $q_\psi(Z|X)$, is introduced to approximate the true posterior $p(Z|X)$. We maximize ELBO

$$\begin{aligned} \log(p(X)) &\geq \mathbb{E}_{q_\psi(Z|X)}[\log p_\theta(X|Z)] \\ &\quad - \text{KL}(q_\psi(Z|X) \parallel p(Z)), \end{aligned}$$

to optimize the encoder and decoder.

For causal representation learning, we reinterpret the latent vector as a set of causal variables $\mathbf{U} = (U_1, \dots, U_p)$ linked by an unknown DAG. Each conditional distribution is reparametrized as

$$\mathbb{P}(U_i | U_{\text{parent}(i)}) = c_i(U_{\text{parent}(i)}, Z_i)$$

where Z_i is an independent exogenous noise variable, and c_i is the causal mechanism that generates U_i from its parent(s) and Z_i . Under this view, the standard VAE likelihood $p_\theta(X|Z)$ factors into a deep SCM

$$\mathbf{Z} \xrightarrow{c} \mathbf{U} \xrightarrow{f_\theta} \mathbf{X}$$

while the ELBO remains the training objective. With this reparameterization, VAE jointly learns the causal graph over \mathbf{U} , the causal mechanisms c_i , and the mixing function f_θ .

Graph-aware encoder

To exploit the rich structural information underlying observable data, we use a GNN as the encoder in our framework. Concretely, we merge all adjacency tensors A_{XX}, A_{XH}, A_{HH} into one untyped edge set \mathbf{A} and build an undirected network (\mathbf{V}, \mathbf{A}) , whose nodes correspond to the entities $\mathbf{V} = (\mathbf{X}, \mathbf{H})$. For each X node, the initial feature h_X is the observable attribute X_v . For each H node without observable features, we initialize the state with an i.i.d. draw from a standard normal such that $h_H \sim N(0, I)$.

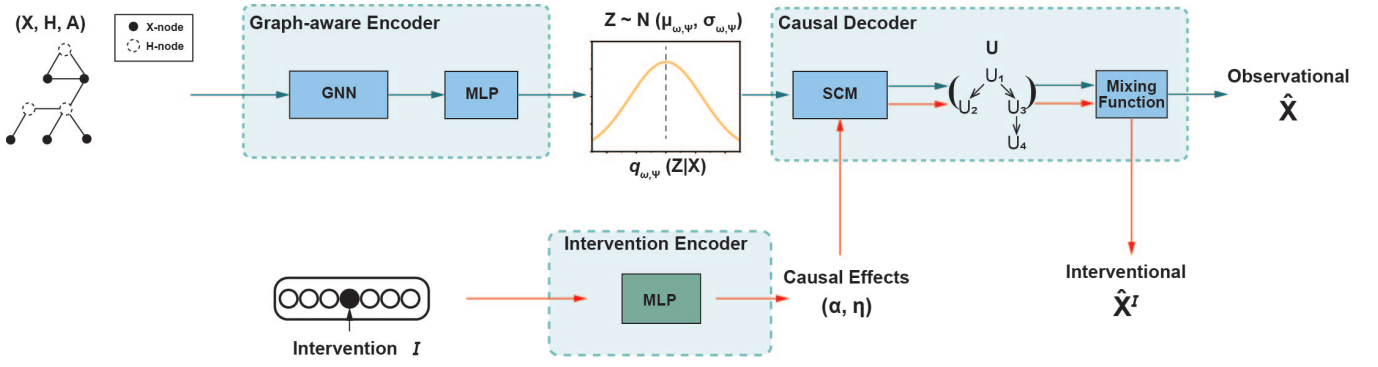


Figure 1: Overview of GRACE-VAE’s architecture. GRACE-VAE consists of a graph-aware encoder, intervention encoder, and a causal decoder. Given entities \mathbf{X} , \mathbf{H} , adjacency structure \mathbf{A} , and intervention I , GRACE-VAE learns a causal directed acyclic graph of the latent variables \mathbf{U} to generate observational $\hat{\mathbf{X}}$ and interventional $\hat{\mathbf{X}}^I$ data.

GRACE-VAE is flexible with any GNN layer propagate neural messages over \mathcal{G} . Here, we instantiate a GraphSAGE layer (Hamilton, Ying, and Leskovec 2017) for concreteness, but we perform experiments on other types of GNN layers as well. In GraphSAGE, each node is assumed to have the following representation:

$$\hat{h}_v = \sigma \left(W_{\text{self}} h_v + W_{\text{nbr}} \frac{1}{|\mathcal{N}(v)|} \sum_{u \in \mathcal{N}(v)} h_u \right), \quad v \in V,$$

where $\mathcal{N}(v)$ represents the merged neighbor set of v , W are the learnable weights, and $\sigma(\cdot)$ a non-linear activation. The message passing yields structure-aware embeddings for the X nodes, denoted as $\hat{\mathbf{X}} = \text{GNN}_w(\mathbf{X})$, for the GraphSAGE example, $\hat{\mathbf{X}} = \{\hat{h}_v, v \in \mathbf{X}\}$, which serve as the input to the variational network: $q_{w,\psi}(Z|\mathbf{X}) = \text{MLP}_\psi(\hat{\mathbf{X}})$.

Our encoder incorporates an external network data $(\mathbf{X}, \mathbf{H}, \mathbf{A})$, capturing the rich structural information among entities \mathbf{X}, \mathbf{H} . This graph-aware encoder injects structural context, mediated by both observed and latent neighbors, into the inference over the exogenous noise variables \mathbf{Z} .

Causal decoder and latent DAG

Following Zhang et al. (2023), the generative decoder $p_\theta(X|Z)$ factorizes into consecutive blocks of an SCM and a mixing function that mirror an implicit causal process. Given an observational sample and an intervention I , GRACE-VAE generates a counterfactual sample \hat{x}^I as well as the reconstructive observational sample \hat{x} . These counterfactuals are compared against the true interventional data in the loss, enabling GRACE-VAE to learn both the latent DAG and the causal effects in an end-to-end manner.

Structural Causal Model (SCM). The exogenous noise vector $\mathbf{Z} \sim N(\boldsymbol{\mu}_\psi(\mathbf{X}), \boldsymbol{\sigma}_\psi(\mathbf{X}))$, where $\boldsymbol{\mu}_\psi(\mathbf{X}), \boldsymbol{\sigma}_\psi(\mathbf{X})$ are the mean and standard deviation vectors produced by q_ψ . Each coordinate of the noise vector Z_i , together with the values of its parents, deterministically produces a causal variable $U_i = c_i(U_{\text{parent}(i)}, Z_i), i \in [p]$. The c_i functions for

soft interventions often take flexible forms, such as neural networks or shift functions that depend on $U_{\text{parent}(i)}$, but introduce an altered mechanism rather than a hard fix (Mansidda et al. 2023). However, for simplicity and easy implementation, we consider the simple MLP function. The set $\text{parent}(i)$ is defined by an *upper-triangular* adjacency matrix M_θ that represents the directed edges in DAG G ; sparsity is promoted through the penalty term $-\lambda \|M_\theta\|_1$.

To model an intervention I , an intervention encoder $(a, \eta) = T_\phi(I)$ outputs $a \in \Delta^{p-1}$, a soft one-hot vector where the largest entry selects the target latent node v and η that specifies the new mechanism for the intervention. We then inform an interventional set of mechanisms:

$$c_i^I(U_{\text{pa}(i)}, Z_i) = \begin{cases} c_i(U_{\text{parent}(i)}, Z_i), & i \neq v, \\ g_i^\eta(U_{\text{parent}(i)}, Z_i), & i = v, \end{cases} \quad i \in [p]$$

g_i^η can be an arbitrary learnable function; here we instantiate g_i^η as an additive shift for computational simplicity following Zhang et al. (2023): $g_i^\eta = c_i(U_{\text{parent}(i)}, Z_i) + \eta, \eta \in R$.

Mixing Function. A neural map $f_\theta : \mathbb{R}^p \rightarrow \mathbb{R}^d$ converts the causal vector to the observed space $\mathbf{X} = f_\theta(\mathbf{U})$. The same mixing function f_θ is shared by observational and interventional regimes.

Objective function

GRACE-VAE is trained on both observational data $P(X)$ and K interventional data $P^{I_k}(X), k \in [K]$. The optimization target therefore couples an ELBO term and a distribution-alignment term. The ELBO term maximizes the likelihood of observed samples:

$$L_{w,\theta,\psi}^{\text{ELBO}} := \mathbb{E}_{x \sim P^{\text{Obs}}(X)} [-\mathbb{E}_{q_{w,\psi}(z|x)} [\log p_\theta(x|z)]] + \beta \times \text{KL}(q_{w,\psi}(z|x) \| p(z)).$$

The distribution-alignment term forces the decoder to reproduce each interventional distribution once the corresponding mechanism has been replaced by the intervention encoder. Formally, let $\hat{X}^{I_k} = f_\theta(U^{I_k})$ be the model-

generated counterfactuals:

$$L_{\omega,\theta,\psi,\phi}^{\text{alignment}} := \alpha \sum_{k=1}^K D_{\gamma}(P^{I_k}(X), P_{\omega,\theta,\psi,\phi}(\hat{X}^{I_k})) + \lambda \|M_{\theta}\|_1.$$

D_{γ} is a discrepancy measurement between two distributions. We utilize the Maximum Mean Discrepancy (MMD) loss for numerical stability. An ℓ_1 penalty $\|M_{\theta}\|_1$ is applied to encourage the sparsity of the latent DAG while still being differentiable. The full loss to minimize is expressed as:

$$L_{\omega,\theta,\psi,\phi} = L_{\omega,\theta,\psi}^{\text{ELBO}} + L_{\omega,\theta,\psi,\phi}^{\text{alignment}}$$

where α, β, γ are hyperparameters. This composite loss enables the learning of graph structure, causal mechanisms, and intervention effects within a single optimization loop.

Identifiability guarantee

Recent theoretical results, notably Zhang et al. (2023), have established that causal structures $\langle G, I_1, \dots, I_K \rangle$ can be identified up to an equivalence class under mild assumptions, including conditions on support, linear interventional faithfulness, and conditional dependence. In our setting, the identifiability guarantee still holds under assumptions 1, 2, and 3 in Zhang et al. (2023). GRACE-VAE enriches inference but leaves both the likelihood and the latent causal structure unchanged, so the original identifiability guarantee remains valid. The detailed discussion is in the Appendix.

Experimental Setup

Datasets

We conduct experiments on 3 genetic perturbation datasets: NORMAN, REPLOGLE-SMALL, and REPLOGLE-LARGE.

NORMAN consists of an observational dataset \mathcal{D}_0 with 8,907 unperturbed cells and an interventional dataset with 99,590 perturbed cells. Cells are perturbed using CRISPR-based screens that target one (i.e., single perturbation) or two (i.e., double perturbation) of 105 genes. These interventions are organized into $K = 217$ distinct interventional datasets, $\mathcal{D}_1, \mathcal{D}_2, \dots, \mathcal{D}_K$, each with 50-2000 cells. A cell is represented by a 5000-dimensional vector X that captures the expression of 5000 highly variable genes.

REPLOGLE-SMALL and REPLOGLE-LARGE are derived from a large-scale CRISPR-based screen that targets 2,058 genes (Replogle et al. 2022). REPLOGLE-LARGE consists of an observational dataset \mathcal{D}_0 with 10,691 unperturbed cells and an interventional dataset with 299,694 perturbed cells resulting from single perturbations. Each cell is represented by a 8563-dimensional vector X that captures the expression of 8,563 highly variable genes. At inference, we predict the effects of 414 perturbation targets (i.e., exclude perturbation targets with fewer than 200 cells). While REPLOGLE-LARGE includes all perturbation targets during training, REPLOGLE-SMALL contains only the 414 perturbation targets. As a result, its interventional dataset has 126,807 cells.

We define **structured biological knowledge** as pathway-gene and pathway-pathway associations (Jassal et al. 2020), and physical protein-protein interactions (Li et al. 2024). For NORMAN, the structured context network consists of 2,694

pathway nodes and 5,000 protein nodes. It includes 22,786 edges connecting pathways to proteins, 2,713 edges between pathways, and 6,191 edges representing protein interactions. For both REPLOGLE-LARGE and REPLOGLE-SMALL, the structured context network consists of 2,694 pathway nodes and 8,563 protein nodes. It includes 75,845 edges connecting pathways to proteins, 2,713 edges between pathways, and 102,087 edges representing protein interactions.

Setup

For NORMAN, we randomly select 96 and 64 cells from each single intervention dataset ($\mathcal{D}_1, \dots, \mathcal{D}_{105}$) containing more than 800 cells for the test and validation sets, respectively. All double intervention datasets are exclusively reserved for the test set. For REPLOGLE-LARGE and REPLOGLE-SMALL, we randomly split 10% and 20% for the validation and test sets. The remaining 70% are used for training; only REPLOGLE-LARGE includes the 1,644 perturbation targets with fewer than 200 samples in the train set.

For **baselines**, we evaluate against CMVAE, the state-of-the-art causal discrepancy VAE architecture (Zhang et al. 2023); CMVAE-multihot, a modification of CMVAE in which a multi-hot encoding of biological pathway information (where 1 indicates that any of the genes in a pathway is expressed in the cell, 0 otherwise) is used as additional input features; and VGAE, an ablation of GRACE-VAE with a standard MLP decoder (instead of a causal decoder). In other words, CMVAE does not incorporate structured biological knowledge, unlike CMVAE-multihot (via multihot encoding) and VGAE (via GNN encoder). Due to computational and memory constraints, we do not evaluate CMVAE-multihot on the REPLOGLE-LARGE dataset.

We conduct **ablation** studies that vary the architecture (i.e., GCN (Bhatti et al. 2023), GAT (Veličković et al. 2017), GraphSAGE (Hamilton, Ying, and Leskovec 2017)) and the number of layers $l \in \{1, 3\}$ of the GNN. We also ablate the level of structured context, considering only gene-gene, pathway-gene, and/or pathway-pathway edges.

We use standard **metrics** to compare the ground truth and generated perturbation effects after single or double intervention: Maximum Mean Discrepancy (MMD), R^2 , and Root Mean Squared Error (RMSE). Following prior work (Zhang et al. 2023), we compute these metrics on the differentially expressed genes (DEGs), which exhibit significant changes in expression under interventions.

Refer to the Appendix for implementation details.

Results

We evaluate GRACE-VAE’s performance to answer the following research questions. **R1:** What is the contribution of structured context for predicting the effects of single interventions? **R2:** What is the contribution of structured context for predicting the effects of unseen intervention combinations? **R3:** How do different graph neural networks capture structured context? **R4:** How does the amount of prior knowledge (via structured context) affect performance?

Dataset	Metric	CMVAE	CMVAE-multihot	VGAE	GRACE-VAE
NORMAN	Single R^2	0.9018 \pm 0.0210	0.9338 \pm 0.0098	0.9493\pm0.0123	0.9452\pm0.0108
	Single RMSE	0.4823 \pm 0.0031	0.4753 \pm 0.0057	0.4763 \pm 0.0045	0.4711\pm0.0066
	Single MMD	0.1538 \pm 0.0188	0.1235 \pm 0.0106	0.1075\pm0.0146	0.1138\pm0.0126
	Double R^2	0.7382 \pm 0.0209	0.7844\pm0.0161	0.7168 \pm 0.0640	0.7845\pm0.0241
	Double RMSE	0.5228 \pm 0.0038	0.5175\pm0.0056	0.5404 \pm 0.0095	0.5204 \pm 0.0037
	Double MMD	0.7990 \pm 0.0495	0.7071\pm0.0388	0.8869 \pm 0.1916	0.7090\pm0.0529
REPROGLE-SMALL	Single R^2	0.8318 \pm 0.0108	0.8379 \pm 0.0139	0.8347 \pm 0.0099	0.8388\pm0.0128
	Single RMSE	0.6032 \pm 0.0135	0.5849 \pm 0.0168	0.5772\pm0.0051	0.5869 \pm 0.0115
	Single MMD	0.5414\pm0.0090	0.5610 \pm 0.0223	0.5970 \pm 0.0067	0.5836 \pm 0.0460
REPROGLE-LARGE	Single R^2	0.8346 \pm 0.0194	—	0.8018 \pm 0.0946	0.8493\pm0.0058
	Single RMSE	0.5997 \pm 0.0165	—	0.5875\pm0.0517	0.5948 \pm 0.0094
	Single MMD	0.5251\pm0.0225	—	0.6750 \pm 0.0238	0.5389 \pm 0.0113

Table 1: Experimental results on 3 genetic perturbation datasets: NORMAN, REPROGLE-LARGE and REPROGLE-SMALL. The prefix “single” and “double” for each metric indicate the model’s performance on single or double interventions respectively. REPROGLE-LARGE and REPROGLE-SMALL only include single interventions. CMVAE-multihot is excluded for REPROGLE-LARGE due to computational and memory constraints. Models are run on 10 seeds. The best-performing model(s) are bolded.

R1: Structured context for single interventions

We evaluate the contributions of structured context for predicting the effects of single interventions on NORMAN, REPROGLE-SMALL, and REPROGLE-LARGE.

Across the three datasets, GRACE-VAE outperforms all baselines on R^2 (Table 1). Notably, GRACE-VAE achieves an average R^2 of 0.9452 compared to CMVAE’s 0.9018 on NORMAN (Figure 2 and Appendix Figure 3 show the learned latent programs in the DAG). CMVAE-multihot and VGAE, which also consider structured context, outperform CMVAE with average R^2 of 0.9338 and 0.9493, respectively.

Compared to CMVAE-multihot, GRACE-VAE shows a marked improvement on all metrics. This underscores the effectiveness of explicitly leveraging the topology of network data rather than relying solely on multihot-encoded features. VGAE, an ablation of GRACE-VAE, often achieves comparable RMSE but worse R^2 and MMD.

Overall, it is worth noting that models that consider structured context (GRACE-VAE, CMVAE-multihot, VGAE) outperform those that do not (CMVAE) in most metrics. GRACE-VAE’s strong performance against all baselines (particularly in R^2) demonstrates the advantage of combining structured context via GNNs and causal modeling.

R2: Structured context for double interventions

We assess the contributions of structured context for predicting the effects of double interventions on NORMAN. Importantly, models are trained only on single interventions, and evaluated on unseen double interventions.

For unseen intervention combinations, the structured context learned by GRACE-VAE’s GNN significantly enhances performance (Table 1). Specifically, GRACE-VAE achieves an average R^2 of 0.7845 and MMD of 0.7090, surpassing CMVAE’s average R^2 of 0.7382 and MMD of 0.7990.

GRACE-VAE performs comparably to CMVAE-multihot, emphasizing the benefit of incorporating structured context. Notably, this comparable performance is achieved with a more compact parameterization, as

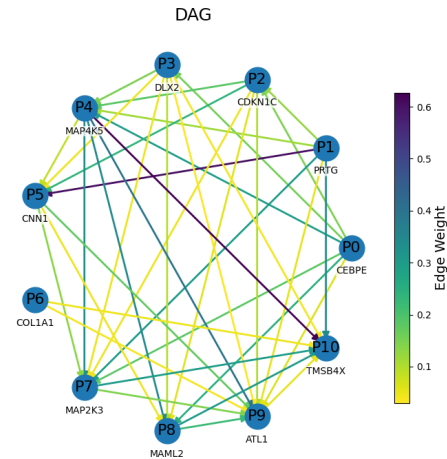


Figure 2: DAG of the learned latent program by GRACE-VAE for NORMAN. Each node is annotated with its most representative gene and edge weights correspond to the absolute values of the learned DAG coefficients.

GRACE-VAE avoids parameter inflation introduced by large multihot encodings (Appendix Table 7). In other words, even with fewer parameters, GRACE-VAE’s encoding of structured knowledge yields comparable predictive performance on double interventions (and stronger performance on single interventions).

Compared to VGAE, the presence of a causal decoder in GRACE-VAE significantly improves its ability to generalize to novel intervention combinations, leading to higher R^2 and lower RMSE and MMD. These results strongly indicate that the synergy between the GNN’s encoding of structured context and the causal decoding in GRACE-VAE is critical for accurately and efficiently modeling and generalizing to complex, previously unseen interventions.

R3: Design of the graph neural network

Any GNN architecture can be flexibly integrated into GRACE-VAE. We evaluate different designs of GNNs on both single and double interventions in NORMAN.

Recall that GRACE-VAE in Table 1 consists of a single GraphSAGE layer. Regardless of the GNN design (Table 2), GRACE-VAE with a 1- or 3-layer GCN, GAT, or GraphSAGE encoder significantly outperform CMVAE (Table 1).

Comparing the different GNN architectures, GRACE-VAE with a GraphSAGE layer has the strongest performance on both single and double interventions. Meanwhile, GCN and GAT have comparable performance with each other on most metrics. It seems that increasing the number of layers does not lead to performance improvement. This indicates that deeper architectures may not necessarily enhance the model’s capacity to learn the underlying mechanisms.

Metric	1-layer GCN	1-layer GAT	3-layer GAT
Single R^2	0.9376 \pm 0.0106	0.9319 \pm 0.0107	0.9302 \pm 0.0133
Single RMSE	0.4744 \pm 0.0073	0.4725 \pm 0.0026	0.4762 \pm 0.0043
Single MMD	0.1242 \pm 0.0113	0.1274 \pm 0.0110	0.1306 \pm 0.0136
Double R^2	0.7593 \pm 0.0252	0.7594 \pm 0.0204	0.7609 \pm 0.0158
Double RMSE	0.5218 \pm 0.0031	0.5192 \pm 0.0016	0.5197 \pm 0.0044
Double MMD	0.7750 \pm 0.0619	0.7912 \pm 0.0531	0.7750 \pm 0.0340

Table 2: Ablation of the GNN architecture in GRACE-VAE, evaluated on NORMAN. The prefix “single” and “double” for each metric indicate model performance on single or double interventions, respectively. Models are run on 10 seeds.

R4: Levels of structured context

While we have demonstrated strong performance gains due to incorporating structured context, we interrogate the contributions to predictive ability by leveraging different levels of structured context. Specifically, we train GRACE-VAE models that consider only gene-gene edges (GG); both gene-gene and pathway-gene edges (GG+PG); or gene-gene, pathway-gene, and pathway-pathway edges (GG+PG+PP). Note that pathway-pathway edges (PP) are limited to those between pathways that are connected to the genes in \mathbf{X} , whereas the pathway-pathway edges learned by GRACE-VAE in Table 1 are between all known pathways.

Introducing progressively richer edge information markedly boosts GRACE-VAE’s performance on predicting the effects of single interventions (Tables 3-4). Adding pathway-gene edges increases R^2 and decreases RMSE on NORMAN and REPLOGLE-SMALL, and decreases MMD on NORMAN. Also, the performance gains plateau (rather than reverse) when pathway-pathway edges are included.

The benefit of adding more structured context is less clear for GRACE-VAE’s performance on predicting the effects of unseen intervention combinations (Table 3). R^2 is slightly decreased, accompanied by a minor increase in MMD, when additional edges are included. These results suggest a trade-off between contextual richness and overfitting risk when incorporating higher order pathway-level information.

We retain the complete network data in GRACE-VAE because its net effect across tasks is still favorable. The slight performance decrease in predicting the effects of double interventions remains within acceptable variance. Further, the full biological topology better positions the framework for future settings in which multi-step or higher-order perturbations become essential. Nevertheless, the inclusion of different levels of structured context in GRACE-VAE can be determined based on the domain or dataset.

Metric	GG	GG+PG	GG+PG+PP
Single R^2	0.9327 \pm 0.0205	0.9414 \pm 0.0117	0.9420 \pm 0.0119
Single RMSE	0.4771 \pm 0.0044	0.4766 \pm 0.0034	0.4752 \pm 0.0075
Single MMD	0.1270 \pm 0.0229	0.1186 \pm 0.0091	0.1233 \pm 0.0132
Double R^2	0.7905 \pm 0.0191	0.7852 \pm 0.0175	0.7851 \pm 0.0177
Double RMSE	0.5177 \pm 0.0053	0.5182 \pm 0.0035	0.5188 \pm 0.0050
Double MMD	0.6990 \pm 0.0489	0.7073 \pm 0.0397	0.7094 \pm 0.0362

Table 3: Ablation of the structured context captured by GRACE-VAE, evaluated on NORMAN. The prefix “single” and “double” for each metric indicate model performance on single or double interventions, respectively. Models are run on 10 seeds. GG = gene-gene edges, PG = pathway-gene edges, PP = pathway-pathway edges.

Metric	GG	GG+PG	GG+PG+PP
R^2	0.8326 \pm 0.0112	0.8401 \pm 0.0096	0.8414 \pm 0.0075
RMSE	0.5927 \pm 0.0090	0.5898 \pm 0.0149	0.5900 \pm 0.0112
MMD	0.5624 \pm 0.0091	0.5691 \pm 0.0237	0.5683 \pm 0.0192

Table 4: Ablation of the structured context captured by GRACE-VAE, evaluated on REPLOGLE-SMALL. Models are run on 10 seeds. GG = gene-gene edges, PG = pathway-gene edges, PP = pathway-pathway edges.

Conclusion

In this work, we introduce GRACE-VAE, a novel general framework to learn a latent causal model by leveraging network data (i.e., structured context). It can handle the realistic setting in which the intervened variables are latent and unknown. We demonstrate that leveraging structured context can boost latent DAG recovery and intervention-effect prediction compared to the encoders without any additional knowledge. Comprehensive experiments confirm that GRACE-VAE yields faithful latent DAGs and accurate predictions of unseen interventions. Empirical results show that performance improvement stems from GRACE-VAE’s unique combination of message passing on network data in the encoder and an explicit structural causal layer in the decoder. Compared to models containing either component in isolation, this architecture markedly lowers counterfactual error and superior recovery of true causal effects. Our work has revealed several promising future directions. To capture more complex or nonlinear perturbation effects commonly observed in biological systems, one can consider more flexible formulations of interventions beyond additive shifts,

such as multiplicative effects, mechanism reparameterizations, or nonlinear transformations. Designing mechanisms that integrate higher-order network knowledge (e.g., pathway hierarchies, gene regulatory modules) directly into the causal structure through pathway-aware constraints on the latent graph or considering relational causal models is another open and promising direction.

Identifiability guarantee

The identifiability argument hinges exclusively on the generative side of the model: observables are produced by a full-row-rank polynomial decoder $f : \mathbb{R}^p \rightarrow \mathbb{R}^d$ through $X = f(U)$, with P_U having interior support. Because the GNN layer is added in the variational encoder, it never enters the likelihood and therefore leaves the observational distribution P_X changed. To show that the latent vector remains identifiable up to an affine reparameterization, we include the following assumptions and theorems, adapted from Zhang et al. (2023), for completeness.

Assumption 1 (Full-rank decoder and latent support). *The observable variables $\mathbf{X} \in \mathbb{R}^d$ are generated by a full-row-rank polynomial $f : \mathbb{R}^p \rightarrow \mathbb{R}^d$ via $\mathbf{X} = f(\mathbf{U})$, and the interior of the support of P_U is non-empty.*

Lemma 1 (Identifiability up to linear transformations). *Suppose Assumption 1 holds. Then the latent dimension p is identifiable from the observational distribution P_X ; and any alternative latent representation $\hat{\mathbf{U}}$ that gives the same P_X must satisfy $\hat{\mathbf{U}} = \Lambda \mathbf{U} + b$ for some non-singular matrix $\Lambda \in \mathbb{R}^{p \times p}$ and vector $b \in \mathbb{R}^p$.*

Proof. Let p^* be the smallest integer for which there exist a latent distribution $P_{\hat{U}}$ and a full-row-rank polynomial $\hat{f} : \mathbb{R}^{p^*} \rightarrow \mathbb{R}^d$ such that $\hat{f}(\hat{\mathbf{U}}) \stackrel{d}{=} \mathbf{X}$. Formally,

$$p^* = \min_{\substack{p' \in \mathbb{N} \\ P_{\hat{U}}, \hat{f}}} \left\{ p' : \hat{f} \text{ is full row rank and } P_{\hat{f}(\hat{\mathbf{U}})} = P_X \right\}.$$

- **Polynomial expansion.** Because f and \hat{f} are full-row-rank polynomials, there exist integers ℓ, ℓ^* and full-row-rank matrices $H \in \mathbb{R}^{(p+\dots+p^\ell) \times d}$, $\hat{H} \in \mathbb{R}^{(p^*+\dots+p^{\ell^*}) \times d}$, with vectors $h, \hat{h} \in \mathbb{R}^d$ such that

$$\begin{aligned} f(\mathbf{U}) &= (U, (U^\alpha)_{\alpha=2}, \dots, (U^\alpha)_{\alpha=\ell})H + h, \\ \hat{f}(\hat{\mathbf{U}}) &= (\hat{U}, (\hat{U}^\alpha)_{\alpha=2}, \dots, (\hat{U}^\alpha)_{\alpha=\ell^*})\hat{H} + \hat{h}, \end{aligned}$$

where $(U^\alpha)_{\alpha=k}$ denotes the vector of all degree- k monomials in the components of \mathbf{U} . Since f, \hat{f} is full-rank, H, \hat{H} have full row rank.

- **Relating $\hat{\mathbf{U}}$ and \mathbf{U}** Equality of the two polynomial maps on the common support of X gives

$$\begin{aligned} (U, (U^\alpha)_{\alpha=2}, \dots, (U^\alpha)_{\alpha=\ell})H + h \\ = (\hat{U}, (\hat{U}^\alpha)_{\alpha=2}, \dots, (\hat{U}^\alpha)_{\alpha=\ell^*})\hat{H} + \hat{h}. \end{aligned} \quad (1)$$

Multiplying (1) on the right by the Moore–Penrose pseudoinverse \hat{H}^\dagger (which exists because \hat{H} has full row rank) yields

$$(\hat{U}, (\hat{U}^\alpha)_{\alpha=2}, \dots) = (U, (U^\alpha)_{\alpha=2}, \dots) H \hat{H}^\dagger + (h - \hat{h}) \hat{H}^\dagger.$$

Hence each component of $\hat{\mathbf{U}}$ is a polynomial in the components of \mathbf{U} ; denote this mapping $\hat{\mathbf{U}} = \text{poly}_1(\mathbf{U})$. By symmetry, we also have $\mathbf{U} = \text{poly}_2(\hat{\mathbf{U}})$.

- **Degree-1 for poly.** Because the interior of the support of P_U is non-empty, both compositions $\mathbf{U} \mapsto \text{poly}_2 \circ \text{poly}_1(\mathbf{U})$ and $\hat{\mathbf{U}} \mapsto \text{poly}_1 \circ \text{poly}_2(\hat{\mathbf{U}})$ coincide with the identity map on an open set of \mathbb{R}^p . By the fundamental theorem of algebra for polynomial automorphisms (Fine and Rosenberger 1997), poly_1 and poly_2 must each be of degree 1. Therefore, there exist a non-singular matrix $\Lambda \in \mathbb{R}^{p \times p^*}$ and a vector $b \in \mathbb{R}^p$ such that $\hat{\mathbf{U}} = \Lambda^\top \mathbf{U} + b$.
- **Minimality of p^* .** Because Λ has full column rank, $p \leq p^*$. Conversely, since p^* is the smallest integer by setting $p^* \leq p$. Hence $p^* = p$, completing the proof. \square

Assumption 2 (Linear interventional faithfulness). *Denote $\text{children}_G(i)$, $\text{descend}_G(i)$, $\text{ancestor}_G(i)$ as the children, descendants, and ancestors of i in G . Intervention I with target i satisfies linear interventional faithfulness if for every $j \in i \cup \text{children}_G(i)$ such that $\text{parent}_G(j) \cap \text{descend}_G(i) = \emptyset$, it holds that $\mathbb{P}(U_j + U_S C^T) \neq \mathbb{P}^I(U_j + U_S C^T)$ for all constant vectors $C \in \mathbb{R}^{|S|}$, where $S = [p] \setminus (\{j\} \cup \text{descend}_G(i))$.*

Assumption 3 (Total separation). *For every edge $i \rightarrow j \in G$, there do not exist constants $c_j, c_k \in \mathbb{R}$ for $k \in S$ such that $U_i \perp\!\!\!\perp U_j + c_j U_i \mid \{U_l\}, l \in \text{parent}_G(j) \setminus (S \cup \{i\}), \{U_k + c_k U_i\}_{k \in S}$, where $S = \text{parent}_G(j) \cap \text{descend}_G(i)$.*

Definition 1 (CD-equivalent class). *Let p be the latent dimension. Two triples*

$$\langle \mathbf{U}, G, I_1, \dots, I_K \rangle, \quad \langle \hat{\mathbf{U}}, \hat{G}, \hat{I}_1, \dots, \hat{I}_K \rangle$$

are CD-equivalent if there exist

$$\pi \in S_p, \quad \lambda_i \neq 0, \quad b_i \in \mathbb{R} \quad (i = 1, \dots, p)$$

such that

$$\hat{U}_i = \lambda_i U_{\pi(i)} + b_i, \quad \hat{G} = G_\pi, \quad \hat{I}_k = (I_k)_\pi \quad (k = 1, \dots, K).$$

Theorem 1 (Identifiability of the latent DAG and intervention targets). *Let Assumptions 1, 2, and 3 hold. Denote $\mathcal{D} = \{D^{(0)}\} \cup \{D^{(k)}\}_{k=1}^K$ the union of the observational sample and the K interventional samples generated by the soft single-node interventions $\{I_k\}_{k=1}^K$. Then the triple $\langle G, \mathbf{U}, I_1, \dots, I_K \rangle$ is identifiable from \mathcal{D} up to CD-equivalence; that is, any other triple producing the same distribution over \mathcal{D} must be CD-equivalent to the truth.*

Proof. The general idea of the proof of Theorem 1 follows the following procedures.

- **Latent coordinates up to an affine map.** Lemma 1 and Assumption 1 imply that from the observational distribution P_X alone we can recover a vector $\hat{\mathbf{U}}$ of dimension p such that $\hat{\mathbf{U}} = \Lambda \mathbf{U} + b$ for a non-singular matrix Λ and a vector b . At this stage, the coordinates of $\hat{\mathbf{U}}$ are an unknown affine reparameterization of the true latent coordinates.

- **Pinning down the permutation.** For each intervention I_k we observe the perturbed distribution $P_X^{I_k}$. Assumption 2 guarantees that the only coordinates of \mathbf{U} whose marginal laws change between P_U and $P_U^{I_k}$ are the target node $i = \text{TG}(I_k)$ and its most upstream children. Because the affine map Λ preserves one-to-one correspondence of coordinates, the same pattern of distributional change appears in $\hat{\mathbf{U}}$. Intersecting the K patterns pins down a *unique* permutation of coordinates and leaves only node-wise non-zero scalings. Equivalently, we obtain an upper-triangular $\tilde{\Lambda}$ whose sparsity pattern matches a topological order of G (Lemmas 5, 6, 7, and 8 in Zhang et al. 2023).
- **Orienting every edge of the DAG.** Suppose an edge $i \rightarrow j$ were wrongly reversed. Then there would exist constants c_j, c_k ($k \in \text{parent}(j) \cap \text{descend}(i)$) making $U_i \perp U_j + c_j U_i \mid \{U_\ell\}_{\ell \in \text{parent}(j) \setminus (\{i\} \cup S)}, \{U_k + c_k U_i\}_{k \in S}$, contradicting Assumption 3, which is proved in detail in Theorem 2 (Zhang et al. 2023). Hence each edge has a unique orientation, fixing the entire DAG G . The remaining ambiguity is the coordinate-wise scaling and shift already allowed by CD-equivalence.

Starting from affine-identified $\hat{\mathbf{U}}$, Assumption 2 eliminates permutation freedom, and Assumption 3 uniquely orients every edge, leaving only coordinate-wise non-zero scalings and shifts.

All three steps rely solely on the likelihood $p(X \mid U)$ and on intervention distributions $p^{I_k}(X \mid U)$, neither of which is altered by inserting the deterministic GNN inside the encoder. Thus, every logical implication in the proof in Zhang et al. (2023) remains valid.

Hence, any alternative triple that reproduces the distribution of \mathcal{D} must satisfy the CD-equivalence relations in Definition 1, completing the proof. \square

Implementation details

Models are implemented in PyTorch and PyTorch Geometric. All models are trained on the same data splits across 10 seeds $s \in [1, 10]$ on the validation dataset. Each model is run on one GPU. We independently perform hyperparameter sweeps for each baseline, GNN architecture ablation, and GRACE-VAE. The selection of hyperparameters are: $\alpha_{\max} \in \{8, 10, 12, 15\}$, $\beta_{\max} \in \{2, 3, 4\}$, $\lambda \in \{0.01, 0.001, 0.0001\}$, and $\text{Temp} \in \{4, 5, 6\}$. For REPLOGLE-LARGE, the selection of latent dimensions $p \in \{100, 200, 300\}$. The best hyperparameter configurations are selected based on R^2 , MMD, and RMSE. Table 5 and Table 6 summarize the detailed information for each model. We will explain in detail the meaning of each coefficient in the following paragraphs.

We use a composite loss function consisting of four terms: (1) a reconstruction loss based on log likelihood, (2) a KL divergence regularization, (3) an MMD term to align generated samples with observed data distributions, and (4) a regularization term to encourage sparsity of the latent DAG. The MMD loss is computed using a mixture of Gaussian

kernels with dyadically spaced bandwidths, following Gretton et al. (2012). The base kernel bandwidth is set to $\sigma = 1000$ and the kernel widths are chosen geometrically as $\sigma, 2\sigma, \dots, 2^{\text{kernel_num}-1}\sigma$, with $\text{kernel_num} = 10$. This multi-scale kernel approach helps stabilize training and ensures sensitivity to discrepancies across a range of scales. The coefficients for the MMD loss (α) and KL loss (β) are scheduled during training as follows: α is set to 0 for the first 5 epochs, then linearly increased to α_{\max} over the next half of training, and held constant thereafter. Similarly, β is set to 0 for the first 10 epochs, then increased linearly to β_{\max} by the midpoint of training and kept fixed for the remaining epochs. The coefficient (λ) for sparsity regularization term is fixed throughout the training.

For VAE parametrization, the encoder consists of GNN layer(s) followed by two fully connected layers with 128 hidden units each, while the decoder consists of a DAG layer followed by two fully connected layers with 128 hidden units. We use leaky ReLU activations for the encoder and decoder. Intervention encoding is handled by a neural network T_ϕ that maps each intervention one-hot indicator to a soft one-hot assignment over the latent space. Specifically, for each intervention, T_ϕ outputs logits that are transformed via a softmax with temperature t , i.e., $T_\phi(I)_i = \frac{\exp(t \times T'_\phi(I))_i}{\sum_{j=1}^p \exp(t \times T'_\phi(I))_j}$, where T'_ϕ is a fully connected network. We employ an annealing schedule for the softmax temperature: $t = 1$ for the first half of epochs, and then t is linearly increased to Temp for the remainder.

For all biological datasets, the choice of latent dimension p is guided by the number of unique intervention targets and validated performance. For NORMAN, we set $p = 105$, matching the number of distinct intervention targets. For REPLOGLE-SMALL, we set $p = 414$, correspondingly. For REPLOGLE-LARGE, we conduct a grid search over $p \in \{100, 200, 300\}$ and select the value achieving the best validation performance; in our experiments, $p = 300$ yields the best results. All models are trained using the Adam optimizer with learning rate = 0.001. We use a batch size of 32 and train each model for 100 epochs.

Visualization of Generated Samples

To visualize and compare the fidelity of the generated and ground-truth samples, we aggregate the control cells, ground-truth post-intervention cells, and model-generated samples into a single data matrix. Specifically, we concatenate the control expression matrix X_{ctrl} , the observed intervention data, and the generated outputs, and then construct a unified AnnData object. Each sample is annotated as 'NA' (control), 'Actual Cells' (real samples), or 'Generated Cells' (generated samples).

Dimensionality reduction is performed using PCA followed by UMAP, with the neighborhood graph constructed from the top 50 principal components. This two-step embedding projects the high-dimensional gene expression profiles into two dimensions, enabling direct visual comparison between the distributions of the real (or ground-truth) and generated samples. In each plot, samples are colored according to their label ('Actual Cells', 'Generated Cells',

Dataset	Hyperparameter	GRACE-VAE	CMVAE	CMVAE-multihot	VGAE
NORMAN	Latent dimension	105	105	105	105
	Number of pathways	2694	2694	2694	2694
	α_{\max}	8	12	8	8
	β_{\max}	2	4	3	2
	λ	0.0001	0.001	0.0001	0.0001
	Temp	4	6	4	4
REPLOGLE-SMALL	Latent dimension	414	414	414	414
	Number of pathways	2694	2694	2694	2694
	α_{\max}	12	12	15	12
	β_{\max}	3	2	2	3
	λ	0.0001	0.0001	0.0001	0.0001
	Temp	5	6	6	5
REPLOGLE-LARGE	Latent dimension	300	300	—	300
	Number of pathways	2694	2694	—	2694
	α_{\max}	12	12	—	12
	β_{\max}	3	2	—	3
	λ	0.0001	0.0001	—	0.0001
	Temp	5	6	—	5

Table 5: Best hyperparameter configurations for GRACE-VAE and baselines.

Hyperparameter	1-layer GCN	1-layer GAT	3-layer GAT
Latent dimension	105	105	105
Number of pathways	2694	2694	2694
α_{\max}	8	8	8
β_{\max}	2	4	3
λ	0.001	0.0001	0.0001
Temp	5	6	5

Table 6: Best hyperparameter configurations for each GNN architecture ablation, evaluated on NORMAN.

or 'NA'). We provide both an overall UMAP for all interventions as well as per-target UMAPs that highlight each single or double gene intervention individually. These visualizations enable qualitative assessment of how closely the generated samples match the true data distributions across various perturbation scenarios.

In our visual analyses, we focus on comparing GRACE-VAE and CMVAE, as these two models are representative of structured and unstructured approaches, respectively. By concentrating on these methods, we aim to highlight the impact of incorporating structured network knowledge while maintaining clarity in our figures.

Figure 4 presents a comprehensive comparison between GRACE-VAE and CMVAE, showing both generated and real samples for all single and double interventions. Both models can broadly capture the effects of interventions. Figures 5 and 6 provide a detailed comparison for each of the 14 single interventions in the NORMAN test set, illustrating close alignment between the generated and true sample distributions for both models. Notably, for certain interventions such as CEBPE and BAK1, GRACE-VAE achieves a noticeably closer match to the experimental data. Overall, by leveraging integrated network knowledge, GRACE-

VAE consistently outperforms CMVAE, achieving higher R^2 scores and lower MMD losses across interventions.

Figures 7 and 8 present representative results for double intervention distributions. In many cases, GRACE-VAE more accurately captures the effects of double perturbations compared to CMVAE. However, there are certain double interventions where neither GRACE-VAE nor CMVAE fully recapitulates the true data distribution, highlighting ongoing challenges in modeling complex combinatorial effects.

Dataset	GRACE-VAE	CMVAE	CMVAE-multihot	VGAE
NORMAN	1,364,035	1,364,029	1,630,531	1,380,120
REPLOGLE-SMALL	2,639,093	2,639,087	2,983,919	2,574,220
REPLOGLE-LARGE	2,498,987	2,498,981	2,843,699	2,500,804

Table 7: Number of parameters in GRACE-VAE and baselines.

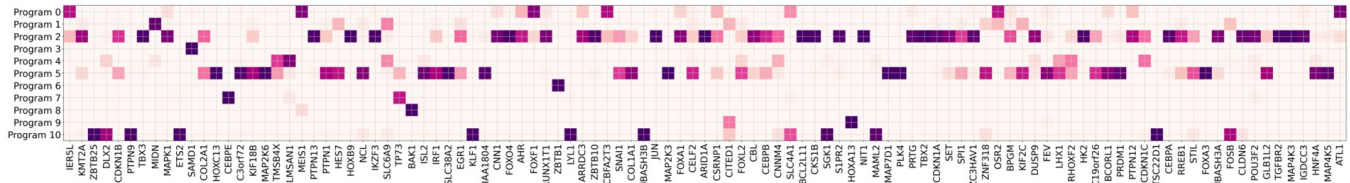


Figure 3: A detailed visualization of the latent program for NORMAN, illustrating for each latent program the full set of associated target gene.

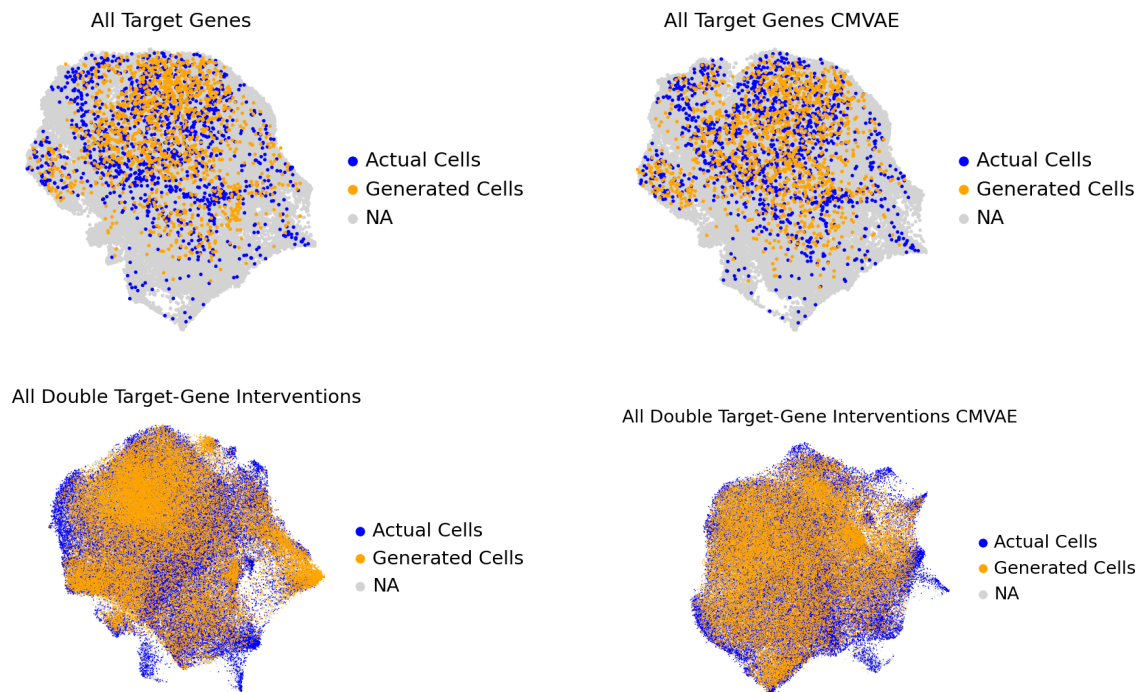


Figure 4: Comparison of generated sample distributions under all single and all double interventions. We visualize the generated samples by GRACE-VAE (left) and CMVAE (right), alongside the actual perturbed cell distributions.



Figure 5: Comparison of generated samples (yellow) versus actual (or ground-truth) observed samples (blue) under single perturbations. Each row corresponds to two pairs; each pair consists of GRACE-VAE (left) and CMVAE (right) alongside the actual perturbed cell distributions.

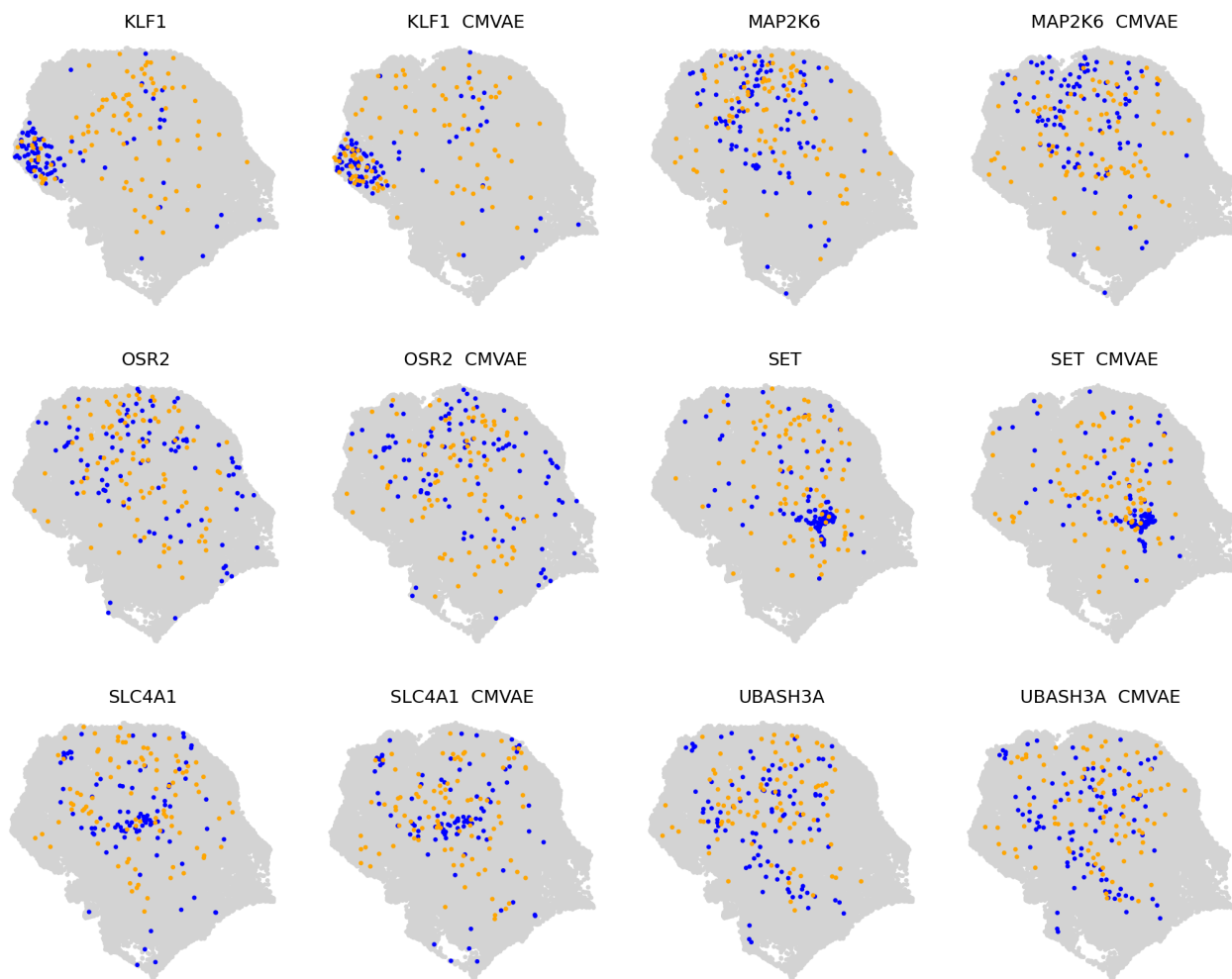


Figure 6: Comparison of generated samples (yellow) versus actual (or ground-truth) observed samples (blue) under single perturbations. Each row corresponds to two pairs; each pair consists of GRACE-VAE (left) and CMVAE (right) alongside the actual perturbed cell distributions.

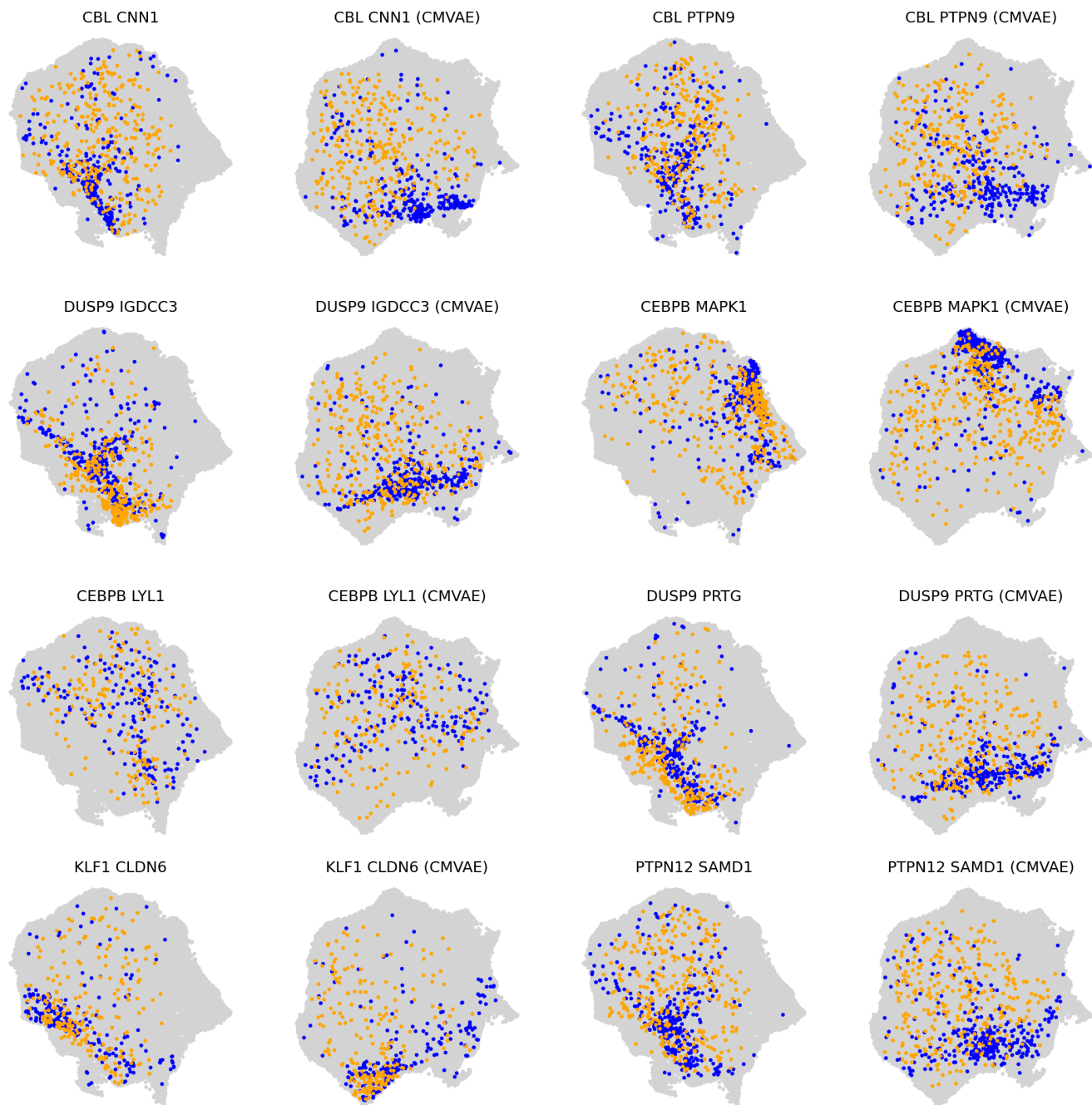


Figure 7: Comparison of generated samples (yellow) versus actual (or ground-truth) observed samples (blue) under double interventions. Each row corresponds to two pairs; each pair consists of GRACE-VAE (left) and CMVAE (right) alongside the actual perturbed cell distributions.

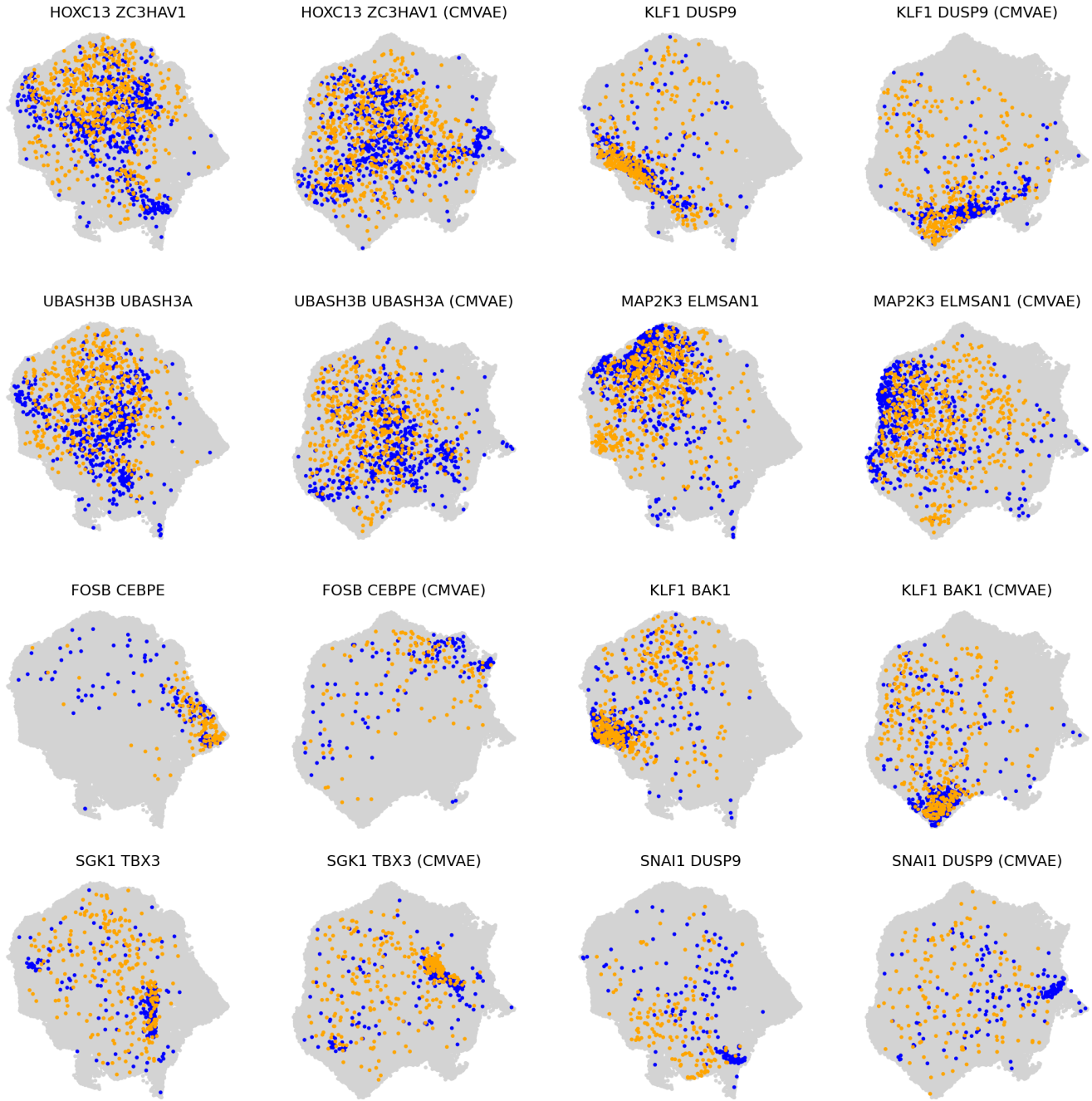


Figure 8: Comparison of generated samples (yellow) versus actual (or ground-truth) observed samples (blue) under double interventions. Each row corresponds to two pairs; each pair consists of GRACE-VAE (left) and CMVAE (right) alongside the actual perturbed cell distributions.

References

- Bhatti, U. A.; Tang, H.; Wu, G.; Marjan, S.; and Hussain, A. 2023. Deep learning with graph convolutional networks: An overview and latest applications in computational intelligence. *International Journal of Intelligent Systems*, 2023(1): 8342104.
- Brehmer, J.; De Haan, P.; Lippe, P.; and Cohen, T. S. 2022. Weakly supervised causal representation learning. *Advances in Neural Information Processing Systems*, 35: 38319–38331.
- Buchholz, S.; Rajendran, G.; Rosenfeld, E.; Aragam, B.; Schölkopf, B.; and Ravikumar, P. 2024. Learning linear causal representations from interventions under general nonlinear mixing. *Advances in Neural Information Processing Systems*, 36.
- Chickering, D. M. 2002. Optimal structure identification with greedy search. *Journal of machine learning research*, 3(Nov): 507–554.
- Cussens, J. 2020. GOBNILP: Learning Bayesian network structure with integer programming. In *International Conference on Probabilistic Graphical Models*, 605–608. PMLR.
- Feng, J.; Zhang, L.; and Yang, L. 2023. Concept-free causal disentanglement with variational graph auto-encoder. *arXiv preprint arXiv:2311.10638*.
- Fine, B.; and Rosenberger, G. 1997. *The fundamental theorem of algebra*. Springer Science & Business Media.
- Gretton, A.; Borgwardt, K. M.; Rasch, M. J.; Schölkopf, B.; and Smola, A. 2012. A kernel two-sample test. *The journal of machine learning research*, 13(1): 723–773.
- Hamilton, W.; Ying, Z.; and Leskovec, J. 2017. Inductive representation learning on large graphs. *Advances in neural information processing systems*, 30.
- Higgins, I.; Amos, D.; Pfau, D.; Racaniere, S.; Matthey, L.; Rezende, D.; and Lerchner, A. 2018. Towards a definition of disentangled representations. *arXiv preprint arXiv:1812.02230*.
- Higgins, I.; Matthey, L.; Pal, A.; Burgess, C. P.; Glorot, X.; Botvinick, M. M.; Mohamed, S.; and Lerchner, A. 2017. beta-vae: Learning basic visual concepts with a constrained variational framework. *ICLR (Poster)*, 3.
- Jassal, B.; Matthews, L.; Viteri, G.; Gong, C.; Lorente, P.; Fabregat, A.; Sidiropoulos, K.; Cook, J.; Gillespie, M.; Haw, R.; et al. 2020. The reactome pathway knowledgebase. *Nucleic acids research*, 48(D1): D498–D503.
- Khemakhem, I.; Monti, R.; Leech, R.; and Hyvarinen, A. 2021. Causal autoregressive flows. In *International conference on artificial intelligence and statistics*, 3520–3528. PMLR.
- Kipf, T. N.; and Welling, M. 2016. Variational graph auto-encoders. *arXiv preprint arXiv:1611.07308*.
- Kong, L.; Huang, B.; Xie, F.; Xing, E.; Chi, Y.; and Zhang, K. 2023. Identification of nonlinear latent hierarchical models. *Advances in Neural Information Processing Systems*, 36: 2010–2032.
- Kumar, A.; Sattigeri, P.; and Balakrishnan, A. 2017. Variational inference of disentangled latent concepts from unlabeled observations. *arXiv preprint arXiv:1711.00848*.
- Li, M. M.; Huang, Y.; Sumathipala, M.; Liang, M. Q.; Valdeolivas, A.; Ananthakrishnan, A. N.; Liao, K.; Marbach, D.; and Zitnik, M. 2024. Contextual AI models for single-cell protein biology. *Nature Methods*, 21(8): 1546–1557.
- Lippe, P.; Magliacane, S.; Löwe, S.; Asano, Y. M.; Cohen, T.; and Gavves, S. 2022. Citris: Causal identifiability from temporal intervened sequences. In *International Conference on Machine Learning*, 13557–13603. PMLR.
- Massidda, R.; Geiger, A.; Icard, T.; and Bacciu, D. 2023. Causal abstraction with soft interventions. In *Conference on Causal Learning and Reasoning*, 68–87. PMLR.
- Pearl, J. 2000. *Causality: Models, Reasoning, and Inference*. Cambridge University Press.
- Raskutti, G.; and Uhler, C. 2018. Learning directed acyclic graph models based on sparsest permutations. *Stat*, 7(1): e183.
- Replogle, J. M.; Saunders, R. A.; Pogson, A. N.; Hussmann, J. A.; Lenail, A.; Guna, A.; Mascibroda, L.; Wagner, E. J.; Adelman, K.; Lithwick-Yanai, G.; et al. 2022. Mapping information-rich genotype-phenotype landscapes with genome-scale Perturb-seq. *Cell*, 185(14): 2559–2575.
- Sanchez-Martin, P.; Rateike, M.; and Valera, I. 2021. Vaca: Design of variational graph autoencoders for interventional and counterfactual queries. *arXiv preprint arXiv:2110.14690*.
- Solus, L.; Wang, Y.; and Uhler, C. 2021. Consistency guarantees for greedy permutation-based causal inference algorithms. *Biometrika*, 108(4): 795–814.
- Squires, C.; Seigal, A.; Bhate, S. S.; and Uhler, C. 2023. Linear causal disentanglement via interventions. In *International Conference on Machine Learning*, 32540–32560. PMLR.
- Suter, R.; Miladinovic, D.; Schölkopf, B.; and Bauer, S. 2019. Robustly disentangled causal mechanisms: Validating

deep representations for interventional robustness. In *International Conference on Machine Learning*, 6056–6065. PMLR.

Tao, H.; Yu, H.; and Li, J. 2024. DeepITE: Designing Variational Graph Autoencoders for Intervention Target Estimation. *Advances in Neural Information Processing Systems*, 37: 89978–90008.

Varici, B.; Acarturk, E.; Shanmugam, K.; Kumar, A.; and Tajer, A. 2023. Score-based causal representation learning with interventions. *arXiv preprint arXiv:2301.08230*.

Veličković, P.; Cucurull, G.; Casanova, A.; Romero, A.; Lio, P.; and Bengio, Y. 2017. Graph attention networks. *arXiv preprint arXiv:1710.10903*.

Yang, M.; Liu, F.; Chen, Z.; Shen, X.; Hao, J.; and Wang, J. 2021. Causalvae: Disentangled representation learning via neural structural causal models. In *Proceedings of the IEEE/CVF conference on computer vision and pattern recognition*, 9593–9602.

Zhang, J.; Greenewald, K.; Squires, C.; Srivastava, A.; Shanmugam, K.; and Uhler, C. 2023. Identifiability guarantees for causal disentanglement from soft interventions. *Advances in Neural Information Processing Systems*, 36: 50254–50292.

Zhu, X.; Xu, C.; and Tao, D. 2021. Commutative lie group vae for disentanglement learning. In *International Conference on Machine Learning*, 12924–12934. PMLR.